Available online at www.sciencedirect.com
SCIENCE DIRECT®
Journal of Sound and Vibration 282 (2005) 163–178
JOURNAL OF SOUND AND VIBRATION
www.elsevier.com/locate/jsvi

# Toward global modelling approaches for dynamic analyses of rotating assemblies of turbomachines

Eric Chatelet*, Flavio D'Ambrosio, Georges Jacquet-Richardet

*Laboratoire de Dynamique des Machines et des Structures, UMR CNRS 5006, Bâtiment Jean d'Alembert, 8 rue des sciences, Institut National des Sciences Appliquées, 69 621 Villeurbanne, France*

Received 14 April 2003; accepted 16 February 2004
Available online 13 October 2004

**Abstract**

It is now increasingly necessary to predict accurately, at the design stage and without excessive computer costs, the dynamic behavior of rotating parts of turbomachines, in order to be able to avoid resonant conditions at operating speeds. Classical approaches are based on different uncoupled models. For example, rotordynamics deals with the shaft behavior while bladed assemblies dynamics deals with wheels, and the possibility of interaction between those elements is generally not analyzed.

In this study, the global non-rotating mode shapes of flexible bladed disc–shaft assemblies are used in a modal analysis method for calculating the dynamic characteristics (frequencies and mode shapes) of the corresponding rotating system. The non-rotating mode shapes are computed using a finite element cyclic symmetry approach. Rotational effects, such as centrifugal stiffening and gyroscopic effects, are accounted for. All the possible couplings between the flexible parts and every kind of deformations are allowed. The proposed model is applied to a thin-walled composite shaft and to a turbomolecular pump rotating assembly. The results obtained illustrate clearly some of the limitations of classical approaches.


## 1. Introduction

Classical approaches used for the dynamic analysis of shaft lines of turbomachines are based on different uncoupled models. For example, the rotordynamics approach assumes that bladed-disc

*Corresponding author. Tel.: +33-4-72-43-62-40; fax: +33-4-72-43-89-30.
*E-mail address:* eric.chatelet@insa-lyon.fr (E. Chatelet).

0022-460X/$ - see front matter © 2004 Elsevier Ltd. All rights reserved.
doi:10.1016/j.jsv.2004.02.035

**Nomenclature**

| | |
|---|---|
| $[\mathbf{C}]$ | mechanical damping and gyroscopic matrix of the whole structure |
| $[\mathbf{C}_{\beta n}]$ | reduced mechanical damping and gyroscopic matrix associated to Fourier order $n$ |
| $[\mathbf{c}_{\beta n}]$ | generalized damping and gyroscopic matrix after modal reduction |
| $E_1$, $E_2$ | longitudinal and transversal Young's moduli |
| $G_{12}$, $G_{13}$, $G_{23}$ | shear moduli |
| $v_{12}$ | Poisson's coefficient |
| $\{\mathbf{F}_c(\Omega^2)\}$ | nodal centrifugal force vector acting on the whole structure |
| $[\mathbf{K}_E]$ | elastic stiffness matrix of the whole structure |
| $[\mathbf{K}_{E\beta n}]$ | reduced elastic stiffness matrix associated to Fourier order $n$ |
| $[\mathbf{K}_G]$ | geometric stiffness matrix of the whole structure |
| $[\mathbf{K}_{G\beta n}]$ | reduced geometric stiffness matrix associated to Fourier order $n$ |
| $[\mathbf{k}_{\beta n}]$ | generalized stiffness matrix after modal reduction |
| $[\mathbf{M}]$ | mass matrix of the whole structure |
| $[\mathbf{M}_{\beta n}]$ | reduced mass matrix associated to Fourier order $n$ |
| $[\mathbf{m}_{\beta n}]$ | generalized mass matrix after modal reduction |
| $[\Omega^2\mathbf{M}_G]$ | supplementary stiffness matrix of the whole structure |
| $[\Omega^2\mathbf{M}_{G\beta n}]$ | reduced supplementary stiffness matrix associated to Fourier order $n$ |
| $[\bar{\mathbf{M}}]$, $[\bar{\mathbf{C}}]$, $[\Omega^2\bar{\mathbf{M}}_G]$, $[\bar{\mathbf{F}}_c]$, $[\bar{\mathbf{K}}_E]$, $[\bar{\mathbf{K}}_G]$ | matrices associated to any sector $p$ (cylindrical co-ordinate system) |
| $N$ | total number of identical jointed sectors |
| $n$ | Fourier order |
| $p$ | index for any cyclic symmetrical sector of the structure ($1 \leqslant p \leqslant N$) |
| $\{\mathbf{q}_{\beta n}\}$ | generalized modal displacements |
| $\beta_n$ | phase shift between the dynamical displacement of adjacent sectors |
| $\dot{\delta}$ | denotes the first derivative (velocity) of quantity "$\delta$" |
| $\ddot{\delta}$ | denotes the second derivative (acceleration) of quantity "$\delta$" |
| $\{\boldsymbol{\delta}\}_s$ | static equilibrium position of the whole structure |
| $\{\boldsymbol{\delta}\}_d$ | dynamic displacement of the whole structure |
| $\{\boldsymbol{\delta}\}_n^c$, $\{\boldsymbol{\delta}\}_n^s$ | cosine and sine terms obtained after decomposition of the dynamic displacement |
| $\{\boldsymbol{\delta}_p\}_d$ | dynamic displacement vector of sector $p$ |
| $\{\boldsymbol{\delta}\}_d^*$ | generalized displacement vector associated to the reference sector obtained after application of the wave propagation relations |
| $\{\bar{\boldsymbol{\delta}}\}_d^*$ | generalized displacement vector of undamped structure at rest associated to the reference sector obtained after application of the wave propagation relations |
| $\omega_r$ | frequency observed in the rotating frame |
| $\omega_f$ | corresponding frequency expressed in the fixed inertial frame |
| $\Omega$ | speed of rotation |
| $[\boldsymbol{\psi}_{\beta n}]$ | modal matrix containing the reduced mode shapes of the undamped structure at rest |
| 1, 2, 3 | orthotropic frame |

flexibility effects are negligible [1] while the bladed disc approach deals with flexible bladed-discs but neglects the effects of shaft flexibility [2]. Those approaches give many advantages and they have proven to be efficient for numerous applications. The main advantages of rotordynamics are given by the one-dimensional (or beam type) behavior hypothesis. The derivation of the associated models is quite simple, lead to low size systems and can account easily for

unsymmetrical supporting structures and global coupling effects. Similarly, when dealing with isolated bladed disc assemblies, efficient models and reduction techniques can be used.

When applied to advanced industrial application, uncoupled approaches may suffer from many disadvantages. They are limited by their basic assumptions and, for example, the rigidity of the wheel shaft attachment is not properly modelled, dynamic interactions between shaft and bladed-disc and between different stages of bladed discs are not considered, shaft cross-sections remain undeformed and are not supposed to be influenced by stress stiffening effects. Some of those limitations are briefly pointed out and discussed below.

1. Shaft modes are mainly beam-like modes (torsional, longitudinal and bending modes). Modes of bladed assemblies are either zero, one, two, or more nodal diameter bending or torsional modes. Inertial coupling between blades and shaft is likely to occur with the zero and one nodal diameter modes of the assembly. Modes with zero nodal diameter are characterized by a resultant loading which is either an axial force (umbrella mode) or an axial torque (torsional mode) and therefore can interact with the longitudinal or torsional shaft deformations, respectively. Modes with one nodal diameter exert a net pitching moment and a shearing force which interacts with the shaft bending modes. Two or more nodal diameter modes are globally reactionless and do not interact with shaft motion. Several studies based on simplified models have been conducted to illustrate the influence of coupling effects within rotating blade–disc–shaft systems [3–10]. The interest in axisymmetrical theory for fully three-dimensional rotordynamic analyses has been demonstrated by Geradin and Kill [11] for critical speed and stability. Geradin and Kill [11] used a component mode method to reduce computational effort. Stephenson and Rouch [12] also proposed an axisymmetrical formulation, but associated with a Guyan reduction technique.
2. When shafts are thick and long, only longitudinal bending or torsional deformations need to be considered. On the other hand, when the structure becomes thin-walled, deformation of the sections should also be considered. These deformations have a significant effect on classical modes and are fully associated with ring-type modes. Furthermore, the effect of rotation on thin tubes, used for example in high-speed centrifugal separators, is significant [13,14].
3. The behavior of composite rotors is usually studied using the equivalent modulus beam approach, where equivalent longitudinal and in-plane shear moduli are obtained from the classical laminate theory and then used within conventional beam models. This approach can lead to significant discrepancies [15–17].

The main problem in the construction of an overall three-dimensional blade–disc–shaft model, adapted to the analysis of a wide range of realistic structures and cases, lies in the difficulty of treating the complex geometrical configuration and behavior of bladed discs elastically attached to a flexible shaft, within a global analysis accounting for all rotational effects. Applying traditional numerical methods used to analyze rotating systems where both centrifugal and gyroscopic effects are taken into account, to models comprising a large number of degrees of freedom, is almost impossible or at least induces prohibitive computer costs. Therefore, to analyze the whole flexible blade–disc–shaft assembly of real structures, efficient reduction techniques have to be proposed and assessed.

The approach presented here is based on a finite element full modelling of the structure but uses two reduction techniques. First, the dynamic behavior of the rotating structure is written in terms of a set of mode shapes associated with the structure at rest. Second, the structure is supposed to be constituted by identical cyclic symmetrical sectors and the behavior of the whole structure at rest is obtained from a finite element model involving only one of these sectors. This procedure, which leads to considerable computer cost savings, has been previously developed and validated using academic structures [18,19]. The applications considered here are based on actual structures and show that the method is adapted to isolated shafts as well as wheel–shaft assemblies, and can be used whatever the finite element considered (shell, volume, etc). The results obtained illustrate the interest in overall modelling techniques compared to classical approaches when dealing with advanced applications.

The following section gives only a brief summary of the theoretical developments related to this study. More details can be found in Appendix A and full derivations can be found in the associated paper referenced [18].

## 2. Equations of motion

The motion equations, expressed in a body fixed co-ordinate system, of a flexible bladed disc mounted on a flexible shaft rotating at a given uniform angular velocity, can be expressed as

$$[\mathbf{K}_E + \mathbf{K}_G(\{\boldsymbol{\delta}\}_s) - \Omega^2\mathbf{M}_G]\{\boldsymbol{\delta}\}_s = \{\mathbf{F}_c(\Omega^2)\}, \tag{1}$$

$$[\mathbf{M}]\{\ddot{\boldsymbol{\delta}}\}_d + [\mathbf{C}]\{\dot{\boldsymbol{\delta}}\}_d + [\mathbf{K}_E + \mathbf{K}_G(\{\boldsymbol{\delta}\}_s) - \Omega^2\mathbf{M}_G]\{\boldsymbol{\delta}\}_d = \{0\}, \tag{2}$$

where $[\mathbf{M}]$ is the mass matrix, $[\mathbf{C}]$ the mechanical damping and gyroscopic (Coriolis) matrix, $[\mathbf{K}_E]$ the elastic stiffness matrix, $[\mathbf{K}_G]$ the geometric stiffness matrix, $[\Omega^2\mathbf{M}_G]$ the supplementary stiffness matrix and $\{\mathbf{F}_c(\Omega^2)\}$ the nodal centrifugal force vector. $\{\boldsymbol{\delta}\}_s$ is the static equilibrium position of the structure under centrifugal loading and $\{\boldsymbol{\delta}\}_d$ is the small amplitude dynamic displacement around the static position. In order to avoid periodic coefficients within the equations, supporting structures (bearings, etc.) shall be considered as fully axisymmetric. In this case, for a given rotational speed $\Omega$, the solution of the non-linear system (1) using a Newton–Raphson procedure, gives the static displacement vector $\{\boldsymbol{\delta}\}_s$. The stiffness matrix is then known and the dynamic problem can be solved.

When dealing with blade–disc–shaft assemblies, the size of the problem can be reduced if those assemblies are characterized by a rotationally periodic property. In this case, structures are constituted of $N$ identical jointed sectors. The matrices as well as the static displacement vector associated with each sector, expressed in a cylindrical co-ordinate system, are identical. According to the wave propagation theory in periodic media [20], the dynamic displacement vector of the different sectors $p$, $\{\boldsymbol{\delta}_p\}_d$, is related to corresponding generalized quantities associated to a reference sector $\{\boldsymbol{\delta}_n^c\}$, $\{\boldsymbol{\delta}_n^s\}$ by the following phase relations:

$$\{\boldsymbol{\delta}_p\}_d = \{\boldsymbol{\delta}_n^c\}\cos(p-1)\beta_n + \{\boldsymbol{\delta}_n^s\}\sin(p-1)\beta_n \tag{3}$$

with $\beta_n$ taking the discrete values $2\pi n/N$, and

$$\begin{aligned} &n = 0, 1, \ldots N/2 && \text{if } N \text{ is even,} \\ &n = 0, 1, \ldots (N-1)/2 && \text{if } N \text{ is odd.} \end{aligned} \tag{4}$$

Applying the wave propagation relations (3), the dynamic problem (2) is divided into $N/2$ uncoupled systems involving matrices function of the phase parameter $\beta_n$ and associated to the reference sector only [18,20,21]

$$\left[\mathbf{M}_{\beta n}\right]\left\{\ddot{\boldsymbol{\delta}}_{\beta n}\right\}_d + \left[\mathbf{C}_{\beta n}\right]\left\{\dot{\boldsymbol{\delta}}_{\beta n}\right\}_d + \left[\mathbf{K}_{E\beta n} + \mathbf{K}_{G\beta n} - \Omega^2\mathbf{M}_{G\beta n}\right]\left\{\boldsymbol{\delta}_{\beta n}\right\}_d = \{0\}. \tag{5}$$

When dealing with bladed-discs, damping and gyroscopic effects are usually neglected and Eq. (5) becomes a Hermitian system which is solved only once, for an operating speed. In this case, reduction of the system using component mode synthesis methods has been widely used and has shown good efficiency. When dealing with blade–disc–shaft assemblies, gyroscopic effects can no longer be neglected and frequency variations with respect to rotation speed are relatively large. Consequently, it becomes necessary to solve a different complex and non-Hermitian eigenvalue problem for each value of the rotation speed in the operating range. In this case, using only traditional reductions based on component mode synthesis methods leads to a lengthy procedure which is still not computationally efficient.

In the following, we shall show that the analysis cost can be reduced, without appreciable loss of accuracy, provided the rotating mode shapes are written as a linear combination of the corresponding non-rotating mode shapes.

## 3. Reduced dynamic problem

The undamped system at rest ($\Omega = 0$) is first considered. Then Eq. (5) reduces to

$$\left[\mathbf{M}_{\beta n}\right]\left\{\ddot{\bar{\boldsymbol{\delta}}}\right\}_d^* + \left[\mathbf{K}_{E\beta n}\right]\left\{\bar{\boldsymbol{\delta}}\right\}_d^* = \{0\}. \tag{6}$$

The solution of Eq. (6) is traditionally computed after a reduction based on the efficient Craig and Bampton substructuring method [21,22] . This gives the frequencies and mode shapes of the non-rotating system. All the mode shapes calculated are grouped into a modal matrix $[\boldsymbol{\psi}_{\beta_n}]$ used for the reduction of the rotating system. Assuming that

$$\{\boldsymbol{\delta}\}_d^* = \left[\boldsymbol{\psi}_{\beta n}\right]\left\{\mathbf{q}_{\beta n}\right\} \tag{7}$$

Eq. (5) becomes

$$\left[\mathbf{m}_{\beta n}\right]\left\{\ddot{\mathbf{q}}_{\beta n}\right\} + \left\lfloor\mathbf{c}_{\beta n}\right\rfloor\left\{\dot{\mathbf{q}}_{\beta n}\right\} + \left\lfloor\mathbf{k}_{\beta n}\right\rfloor\left\{\mathbf{q}_{\beta n}\right\} = \{\mathbf{0}\} \tag{8}$$

with

$$\begin{aligned} \left[\mathbf{m}_{\beta n}\right] &= \left[\boldsymbol{\psi}_{\beta n}\right]^{\mathrm{t}}\left[\mathbf{M}_{\beta n}\right]\left[\boldsymbol{\psi}_{\beta n}\right], \\ \left[\mathbf{c}_{\beta n}\right] &= \left[\boldsymbol{\psi}_{\beta n}\right]^{\mathrm{t}}\left[\mathbf{C}_{\beta n}\right]\left[\boldsymbol{\psi}_{\beta n}\right], \\ \left[\mathbf{k}_{\beta n}\right] &= \left[\boldsymbol{\psi}_{\beta n}\right]^{\mathrm{t}}\left[\mathbf{K}_{E\beta n} + \mathbf{K}_{G\beta n} - \Omega^2\mathbf{M}_{G\beta n}\right]\left[\boldsymbol{\psi}_{\beta n}\right]. \end{aligned} \tag{9}$$

The solution of Eqs. (6) and (8) is computed for all the possible values of the phase parameter $\beta_n$ given by Eq. (4). The frequencies of the rotating system are obtained directly. The corresponding mode shapes can be obtained after applying the two successive transformations, Eqs. (7) and (3), to the calculated eigenvectors. In order to be able to identify possible resonance points, frequencies are calculated for the whole operating range of the structure and the results classically reported on a Campbell diagram, which illustrate the dependence of natural frequencies on rotor speed $\Omega$. When using the proposed analysis method, the non-rotating mode shapes of the assembly are calculated only once. Then, the following steps are involved for each rotation speed considered:

- the static problem Eq. (1) is solved,
- the dynamic problem Eq. (5) is reduced according to Eq. (7),
- the reduced system Eq. (8) is solved.

Compared to traditional procedures, the computer cost saving is considerable and allows precise analyses of complex industrial structures using workstations. The accuracy of the method has been validated in Refs. [18,19].

## 4. Application to a thin-walled composite shaft

Because of the specific strength and stiffness of high-performance fiber-reinforced composite materials, attempts are made to replace metallic shafts by composite shafts in specific applications such as, for example, driveshafts for helicopters, cars and jet engines, or centrifugal separator cylindrical tubes [23–26]. These materials provide direct advantages in terms of weight saving, placement of critical speeds, smoother and supercritical operations. They also give the designer the possibility to obtain a predetermined behavior, without weight or geometry penalties, by changing the arrangement of the different composite layers: i.e., orientation, number of plies [26,27].

The application considered first is a simply supported thin-walled tube with two lateral inner discs at both ends (Fig. 1). The shaft length is $L = 1.5\,\text{m}$, its outer diameter is $D = 0.09\,\text{m}$ and its wall thickness is $e = 7.0 \times 10^{-4}\,\text{m}$. The discs lie at a distance of 0.05 m from both ends of the tube, their thickness is $e_d = 3.0 \times 10^{-3}\,\text{m}$ and their inner radius is $r_d = 0.0075\,\text{m}$. The shaft is made of five layers of Boron/Epoxy ($\rho = 1600\,\text{kg/m}^3$, $E_1 = 3.0 \times 10^{11}\,\text{Pa}$, $E_2 = 6.2 \times 10^9\,\text{Pa}$, $G_{12} = G_{13} = G_{23} = 4.1 \times 10^9\,\text{Pa}$ and $v_{12} = 0.26$).

The stacking sequence considered is $[0^\circ, -30^\circ, +30^\circ, 0^\circ, 90^\circ]$, given from the inner to the outer surface of the cylinder. Mechanical damping is neglected.

As shown in Fig. 2 , only $\frac{1}{12}$th ($30^\circ$) of the whole structure is meshed using five elements along the circumference and 36 elements along the length. The two lateral inner discs are meshed using 20 elements each. The resulting mesh, dark sector in Fig. 2, consists of 220 elements and 4019 degrees of freedom.

The finite element chosen here is a multilayered shell element, constructed from the solid isoparametric element with 16 nodes, by applying Reissner–Mindlin cinematical hypotheses [28,29]. The resulting element is geometrically characterized by 16 nodes and cinematically by 8 nodes and 5 degrees of freedom per node. A shear correction coefficient equal to $\frac{5}{6}$ is considered and reduced integration is used to prevent shear locking.

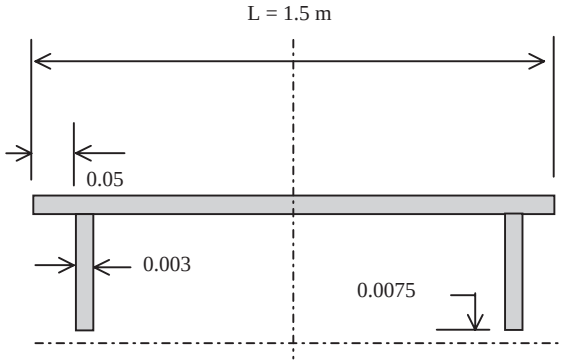


Fig. 1. Cylindrical tube with lateral inner discs.

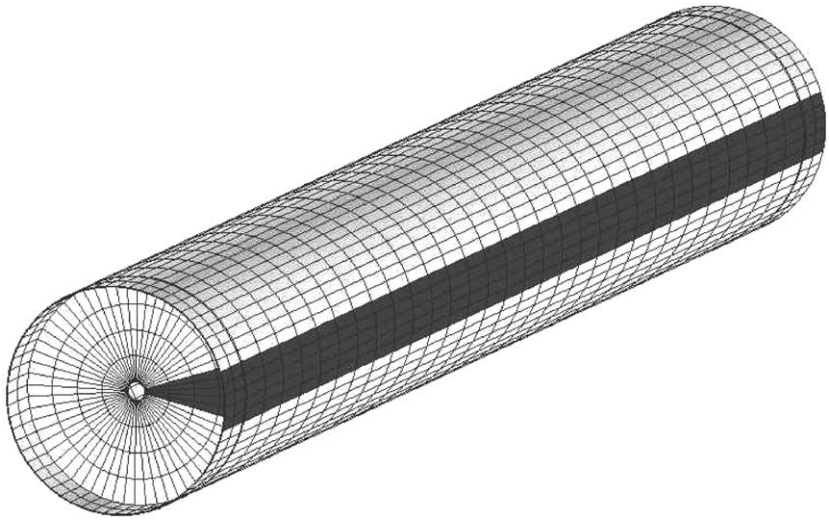

Fig. 2. Cylindrical tube with lateral inner discs only $\frac{1}{12}$th of the mesh (dark portion) is considered by the numerical model.

The three first bending frequencies, obtained using the proposed method for the structure at rest, are reported in Table 1. These values are compared with those computed using ROTORINSA associated with an Equivalent Beam Modulus Approach (EBM) based on Tsaï formulation [17,30]. ROTORINSA [31] is an in-house computer program developed to analyze the dynamic behavior of rotors in bending and based on a beam finite element modelling.

Differences in results are significant and can be explained as follows. First, the laminate theory supposes that the contribution of each layer is independent of its radial position, this hypothesis being only valid for thin-walled shafts with symmetrical sequences. Second, the beam theory does not consider longitudinal shear deformations associated with bending.

Table 1
Composite rotor, comparison of natural frequencies at rest

| Bending modes | ROTORINSA (EBM) (Hz) | 3D model (Hz) | Δ (%) |
|---|---|---|---|
| 1 | 508.4 | 475.4 | 6.7 |
| 2 | 1749.2 | 1446.7 | 18.9 |
| 3 | 3305.7 | 2564.7 | 24 |

Table 2
Composite rotor, first critical speeds

| Critical speeds | ROTORINSA (rev/min) | 3D model (rev/min) | Δ (%) |
|---|---|---|---|
| 1 | 31,820 | 28,570 | 11.4 |
| 2 | 116,625 | 91,660 | 27.2 |

The critical speeds obtained with both three-dimensional and beam models are reported in Table 2. Due to stress stiffening effects, the accuracy of the beam model decreases when rotation speed increases.

## 5. Application to a turbomolecular pump rotor

Turbomolecular pumps are used for gas analysis, leak detection and process monitoring.

This second application is based on the analysis of the rotating assembly of a magnetically levitated turbomolecular pump, designed for semiconductor processes and developed by ALCATEL Vacuum Technology (ATH series). The main dimensions of the rotating assembly, presented in Fig. 3, are: length $L = 0.26\,\mathrm{m}$ and max radius $R = 0.10\,\mathrm{m}$. For this specific application most of the stages are constituted by 24 radial blades mounted on an axisymmetric shaft. One quarter of the structure is presented in Fig. 4, and, as shown in Fig. 5, only a portion of $15^\circ$ ($\frac{1}{24}$th) of the whole assembly is considered by the numerical model. The cyclic-symmetrical sector of the structure is meshed using 1416 isoparametric finite elements with 20 nodes. Damping effects are neglected and the rotor is supposed to be in a free–free configuration. Such a configuration has been validated by comparison of numerical results with experimental results obtained on the running structure. As shown in Eq. (4), the whole behavior of the assembly is obtained through computation of different cases associated with all the possible phase angles between sectors. Shaft modes can occur only with $n = 0$ or 1 ($n = 0$ torsion and longitudinal modes, $n = 1$ bending modes). Modes of the bladed assembly are either zero ($n = 0$), one ($n = 1$), two ($n = 2$), or more nodal diameter bending or torsion modes. Here, only cases involving shaft bending ($n = 1$) will be considered.

As the rotating part is not axisymmetric, results associated with the proposed method are computed with respect to the rotating frame while results of classical rotordynamics approaches

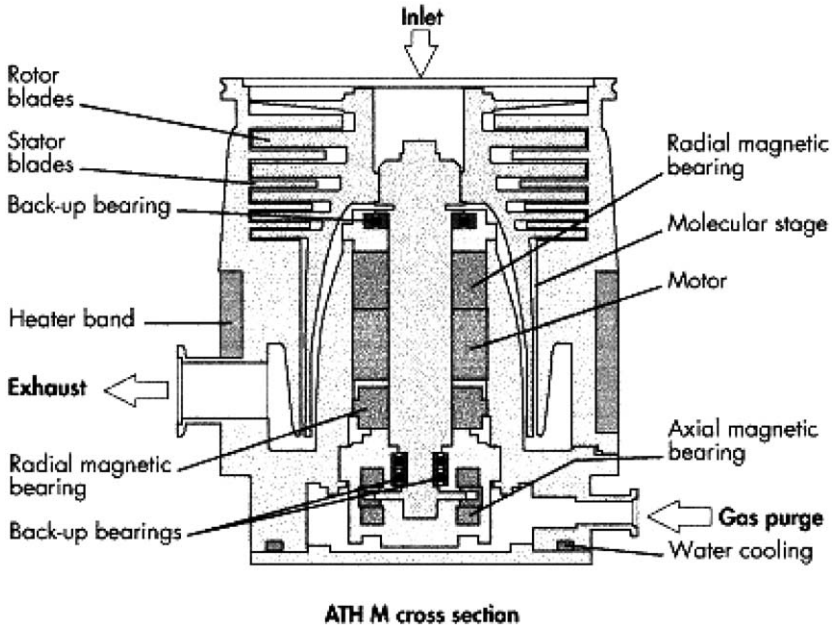


Fig. 3. Turbomolecular pump.

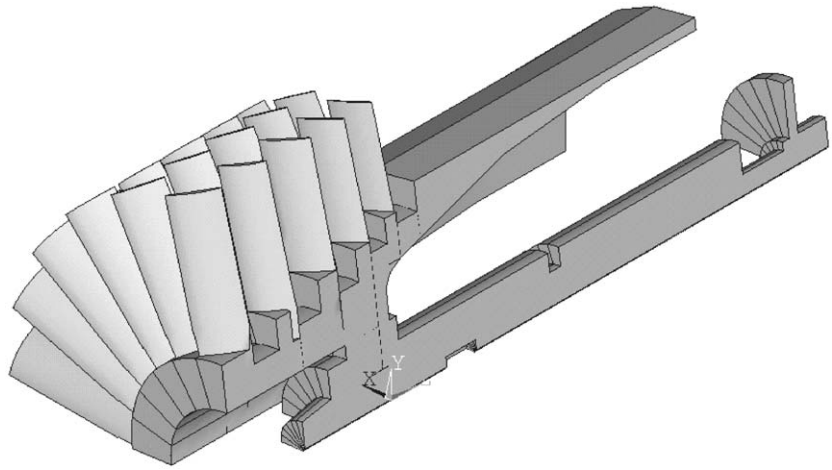

Fig. 4. Representation of $\frac{1}{4}$th of the rotating assembly.

are usually given in the fixed inertial frame. When dealing with bending modes of rotors, the transformation from rotating to non-rotating frames is a function of the nature of the mode which can be a forward whirling mode, whirl in the direction of rotation, or a backward whirling mode, whirl against the direction of rotation. Such a transformation is given by the simple

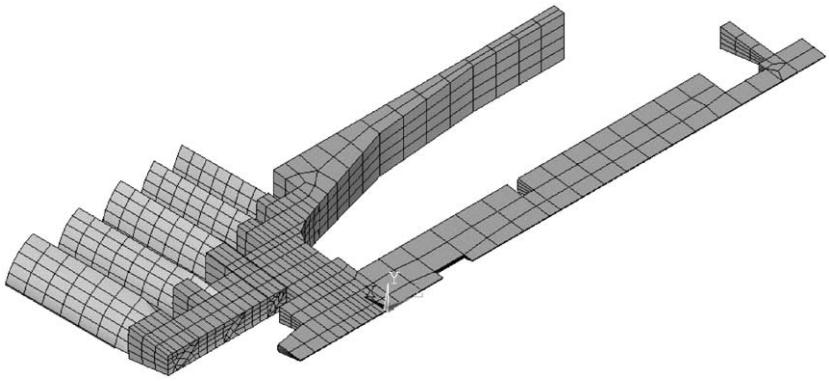

Fig. 5. Finite element mesh of the cyclic sector.

relations:

$$\begin{aligned} \omega_f &= |\omega_r + \Omega| \quad \text{for a forward whirl,} \\ \omega_f &= |\omega_r - \Omega| \quad \text{for a backward whirl,} \end{aligned} \tag{10}$$

where $\omega_r$ is the frequency observed in the rotating frame and $\omega_f$ is the corresponding frequency expressed in the fixed inertial frame.

Three set of results are computed and compared in order to illustrate coupling effects between the different flexible components of the assembly. The first set is associated to the flexible-blade flexible-shaft model (Fig. 6), the second one to a rigid-blade flexible-shaft model (Fig. 7) and the third one to a flexible-blade rigid-shaft model (Fig. 8). The results obtained are summarized in Tables 3 and 4.

At rest, the first mode is mainly a first shaft bending while the other modes involve motion of the different blade stages. As shown in Table 3, modes 1, 4 and 6 are highly coupled shaft-blade modes while modes 2, 3 and 5 are blade modes with very slight participation of shaft bending.

Coupling is much less pronounced when rotational speed increases. As shown in Table 4 and in Figs. 6 and 8, the effect of blade flexibility on the forward whirling shaft mode decreases as speed increases. At 30,000 rev/min. the associated frequency given by the flexible and rigid blade models is almost identical. The influence of shaft flexibility becomes negligible when considering blade modes beyond 15,000 rev/min. However, the effect of shaft blade coupling remains significant, over the whole rotational range, for the backward branch of the shaft bending mode.

Considering these results it appears that, for the structure considered, the limitations of classical rotordynamics and bladed-disc assembly dynamics approaches concern the whole behavior in the case of relatively low rotational speeds and the backward whirling shaft mode over the entire speed range.

## 6. Conclusion

This paper is directed toward the construction of overall modelling techniques adapted to the prediction of the dynamic behavior of rotating shaft lines. The method proposed considers the

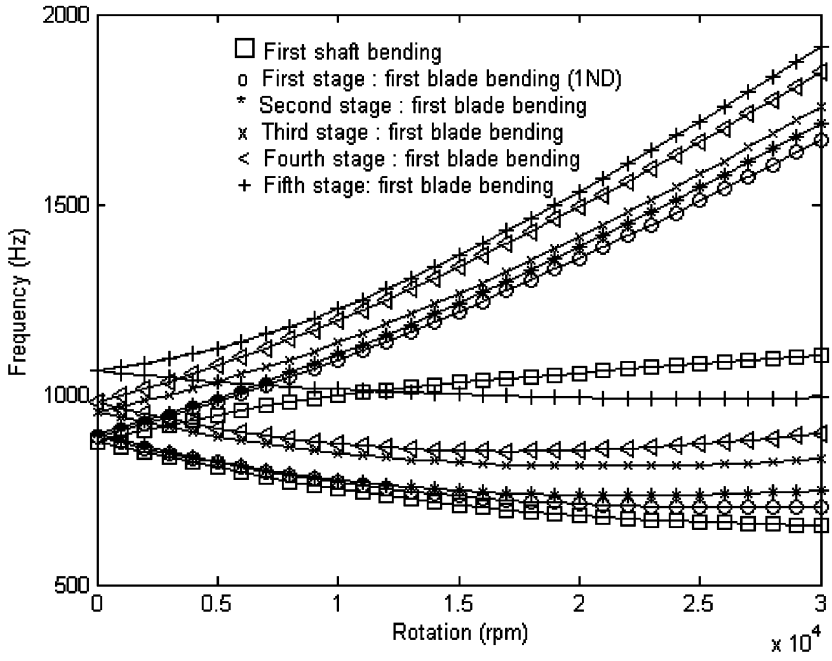


Fig. 6. Campbell diagram in the fixed reference frame—flexible model.

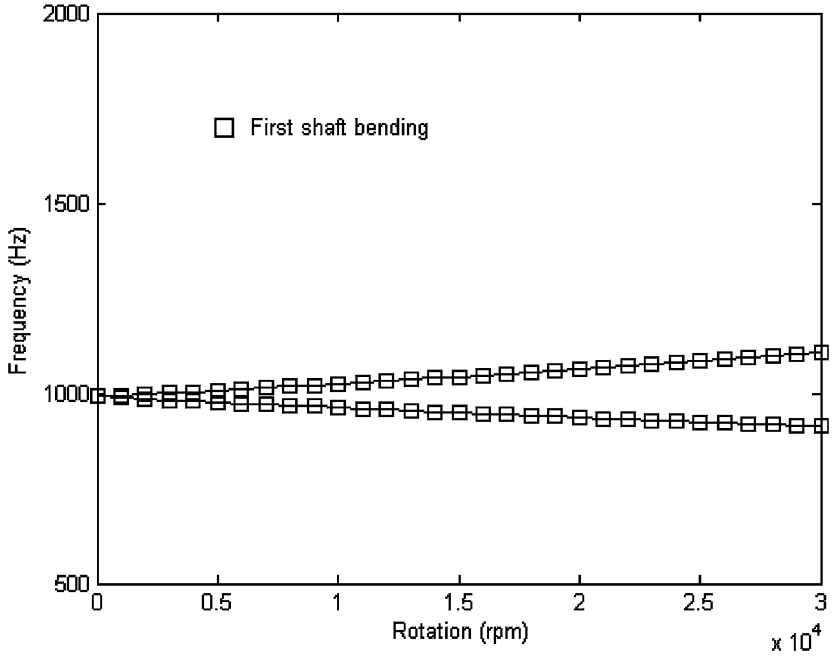


Fig. 7. Campbell diagram in the fixed reference frame—rigid blades model.

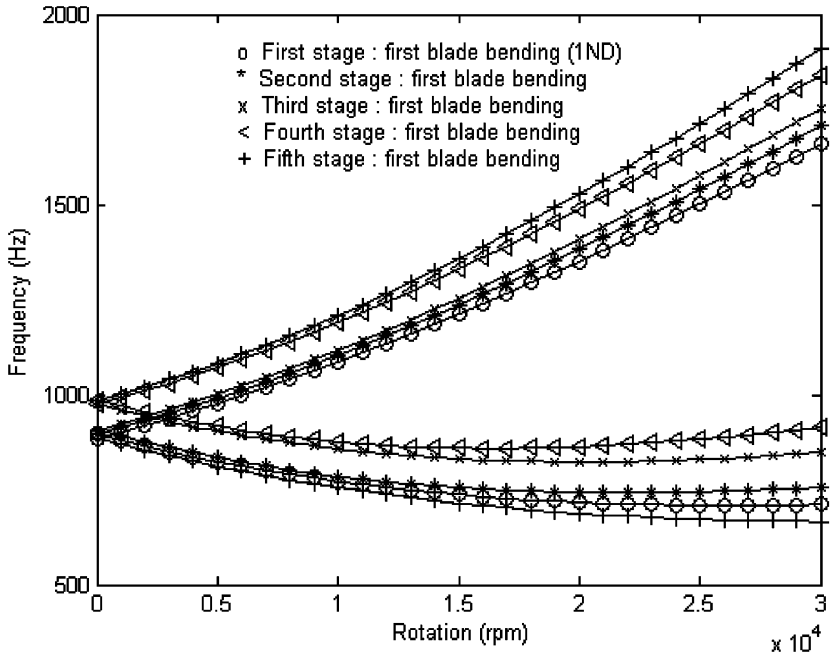


Fig. 8. Campbell diagram in the fixed reference frame—rigid shaft model.

Table 3
Comparison between the flexible model and, respectively, the rigid-blade and rigid-shaft models ($\Omega = 0$ rev/min, $n = 1$)

| No | Flexible blades flexible shaft | Rigid blades flexible shaft | Δ (%) | Flexible blades rigid shaft | Δ (%) |
|---|---|---|---|---|---|
| 1 | 877.0 | 991 | 13.1 | — | — |
| 2 | 890.0 | — | — | 885.0 | −0.5 |
| 3 | 897.0 | — | — | 897.0 | 0.0 |
| 4 | 953.0 | — | — | 908.0 | −4.8 |
| 5 | 980.0 | — | — | 975.0 | −0.5 |
| 6 | 1064.0 | — | — | 985.0 | −7.4 |

complex shape of the structure as well as the complex effects generated by rotation, in a global model taking into account all the possible displacements and coupling between the different flexible parts. A considerable attention has been given to reduction in the size of the system, in order to allow precise computations of real structures without excessive computer costs.

The main interest lies in the applications which illustrate the capacity of such methods to deal with wheel–shaft assemblies. The results obtained show that the behavior of such systems may be poorly modelled using traditional modelling techniques based on one-dimensional beam approaches.

Table 4
Comparison between the flexible model and, respectively, the rigid-blade and rigid-shaft models ($\Omega = 30,000$ rev/min, $n = 1$)

| No | Flexible blades flexible shaft | Rigid blades flexible shaft | Δ (%) | Flexible blades rigid shaft | Δ (%) |
|---|---|---|---|---|---|
| 1 | 657.0 | — | — | 666.0 | 1.4 |
| 2 | 704.0 | — | — | 711.0 | 1.0 |
| 3 | 748.0 | — | — | 756.0 | 1.1 |
| 4 | 829.0 | — | — | 848.0 | 2.3 |
| 5 | 896.0 | — | — | 915.0 | 2.1 |
| 6 | 992.0 | 914.0 | −7.9 | — | — |
| 7 | 1104.0 | 1106.0 | 0.2 | — | — |
| 8 | 1669.0 | — | — | 1659.0 | −0.6 |
| 9 | 1713.0 | — | — | 1708.0 | −0.3 |
| 10 | 1758.0 | — | — | 1754.0 | −0.2 |
| 11 | 1848.0 | — | — | 1842.0 | −0.3 |
| 12 | 1917.0 | — | — | 1909.0 | −0.4 |

## Acknowledgments

The authors wish to thank ALCATEL Vacuum Technology, Annecy, France and especially Mr. Dauvillier for providing the vacuum pump application.

## Appendix A

The structures considered are composed of $N$ identical sectors. Matrices $([\bar{\mathbf{M}}], [\bar{\mathbf{C}}], [\Omega^2\bar{\mathbf{M}}_G], [\bar{\mathbf{F}}_c], [\bar{\mathbf{K}}_E], [\bar{\mathbf{K}}_G])$ associated to all the sectors, expressed in a cylindrical coordinate system, are identical. Thus Eqs. (1) and (2) come from the application of Lagrange's equations to the expression of kinetic ($T$) and potential ($U$) energies associated to the rotating system

$$T = \sum_{p=1}^{N} \left[ \tfrac{1}{2}\{\dot{\boldsymbol{\delta}}_p\}^{\mathrm{t}}[\bar{\mathbf{M}}]\{\dot{\boldsymbol{\delta}}_p\} + \tfrac{1}{2}\{\dot{\boldsymbol{\delta}}_p\}^{\mathrm{t}}[\bar{\mathbf{C}}]\{\boldsymbol{\delta}_p\} + \tfrac{1}{2}\{\boldsymbol{\delta}_p\}^{\mathrm{t}}[-\Omega^2\bar{\mathbf{M}}_G]\{\boldsymbol{\delta}_p\} + \{\boldsymbol{\delta}_p\}^{\mathrm{t}}[\bar{\mathbf{F}}_c(\Omega^2)] \right], \quad \text{(A.1)}$$

$$U = \sum_{p=1}^{N} \left[ \tfrac{1}{2}\{\boldsymbol{\delta}_p\}^{\mathrm{t}}[\bar{\mathbf{K}}_E]\{\boldsymbol{\delta}_p\} + \tfrac{1}{2}\{\boldsymbol{\delta}_p\}^{\mathrm{t}}[\bar{\mathbf{K}}_G]\{\boldsymbol{\delta}_p\}. \right. \quad \text{(A.2)}$$

The assembly of vectors $\{\boldsymbol{\delta}_p\}$ gives $\{\boldsymbol{\delta}\}$ which contains all the d.o.f. of the whole structure. $\{\boldsymbol{\delta}\}$ is classically decomposed into two parts $\{\boldsymbol{\delta}\}_s$ and $\{\boldsymbol{\delta}\}_d$. $\{\boldsymbol{\delta}\}_s$ , gives the static equilibrium position under centrifugal loading and $\{\boldsymbol{\delta}\}_d$ is the small amplitude dynamic displacement around the static position. This decomposition leads, after linearization of the dynamical part, to the classical systems (1) and (2).

The wave propagation theory in periodic media allows a discrete Fourier series decomposition of the global dynamical displacement along the different cyclic sectors. Thus

$$\{\boldsymbol{\delta}_p\}_d = \sum_{n=0}^{D/2} \{\boldsymbol{\delta}_n^c\} \cos(p-1)\beta_n + \{\boldsymbol{\delta}_n^s\} \sin(p-1)\beta_n, \tag{A.3}$$

where $\beta$ represents the phase shift between sectors, $D$ is $N$ if $N$ is even or $(N-1)$ if $N$ is odd and $\{\boldsymbol{\delta}_n^c\}$, $\{\boldsymbol{\delta}_n^s\}$ are the generalized quantities associated to a reference sector.

Carrying over Eq. (A.3) to the expression of the energies associated to the dynamical problem gives independent terms for all possible values of $n$:

$$T_n = \frac{N^*}{2} \begin{Bmatrix} \boldsymbol{\delta}_n^c \\ \boldsymbol{\delta}_n^s \end{Bmatrix}^{\mathrm{t}} \begin{bmatrix} \bar{\mathbf{M}} & 0 \\ 0 & \bar{\mathbf{M}} \end{bmatrix} \begin{Bmatrix} \boldsymbol{\delta}_n^c \\ \boldsymbol{\delta}_n^s \end{Bmatrix} + \cdots, \tag{A.4}$$

$$U_n = \frac{N^*}{2} \begin{Bmatrix} \boldsymbol{\delta}_n^c \\ \boldsymbol{\delta}_n^s \end{Bmatrix}^{\mathrm{t}} \begin{bmatrix} \bar{\mathbf{K}}_E & 0 \\ 0 & \bar{\mathbf{K}}_E \end{bmatrix} \begin{Bmatrix} \boldsymbol{\delta}_n^c \\ \boldsymbol{\delta}_n^s \end{Bmatrix} + \cdots, \tag{A.5}$$

where $N^* = N$ if $\beta = 0$ or $\beta = \pi$, $N^* = N/2$ otherwise.

Due to relation (A.3), d.o.f.'s associated to the boundaries of the reference sector are not independent and one of these has to be eliminated before application of the Lagrange's equations. Considering that the dynamical displacement of each sector is constituted of $\boldsymbol{\delta}_l$, $\boldsymbol{\delta}_r$ and $\boldsymbol{\delta}_i$ type d.o.f. ($l$, $r$, $i$ represents dof associated to the left boundary, right boundary and internal domain), and writing right boundary d.o.f. as a function of left ones gives, after application of Lagrange's equations, the $N/2$ uncoupled systems (5) where $\{\boldsymbol{\delta}\}_d^* = \langle \boldsymbol{\delta}_{nl}^c, \boldsymbol{\delta}_{ni}^c, \boldsymbol{\delta}_{nl}^s, \boldsymbol{\delta}_{ni}^s \rangle$ and matrices take the following form:

$$[\mathbf{A}_{\beta n}] = \begin{bmatrix} A_{ll} + A_{rr} + (A_{lr} + A_{rl}) \cos\beta & A_{li} + A_{ri} \cos\beta & (A_{lr} + A_{rl}) \sin\beta & -A_{ri} \sin\beta \\ A_{il} + A_{ir} \cos\beta & A_{ii} & A_{ir} \sin\beta & 0 \\ (A_{rl} + A_{lrl}) \sin\beta & A_{ri} \sin\beta & A_{ll} + A_{rr} + (A_{lr} + A_{rl}) \cos\beta & A_{li} + A_{ri} \cos\beta \\ -A_{ir} \sin\beta & 0 & A_{il} + A_{ir} \cos\beta & A_{ii} \end{bmatrix}, \tag{A.6}$$

where $l$, $r$, $i$ are associated to the partition of basic sector matrices according to left, right and internal d.o.f.'s.

## References

[1] M. Lalanne, G. Ferraris, *Rotordynamics Prediction in Engineering*, 2nd Edition, Wiley, New York, 1997.

[2] V. Omprakash, V. Ramamurti, Analysis of bladed disks. A review, *The Shock and Vibration Digest* 20 (11) (1988) 14–21.

[3] J.A. Dopkin, T.E. Shoup, Rotor resonant speed reduction caused by flexibility of disks, *Journal of Engineering for Industry* 96 (4) (1974) 1328–1333.
[4] D.R. Chivers, H.D. Nelson, The natural frequencies and critical speeds of a rotating flexible shaft disc system, *Journal of Engineering for Industry* 97 (1975) 881–886.
[5] N. Klompas, Significance of disk flexing in viscous damped jet engine dynamics, *Journal of Engineering for Power* 100 (1978) 647–654.
[6] J.A. Palladino, J.N. Rossettos, Finite element analysis of the dynamics of flexible disk rotor systems, ASME Paper 82GT240, 1982.
[7] P. Bremand, G. Ferraris, M. Lalanne, Prediction of natural frequencies of flexible shaft disc system, *The Shock and Vibration Bulletin* 56 (2–3) (1986) 71–80.
[8] E.F. Crawley, E.H. Ducharme, D.R. Mokadam, Analytical and experimental investigation of the coupled bladed disk-shaft whirl of a cantilever turbofan, *Journal of Engineering for Gas Turbine and Power* 108 (1986) 567–576.
[9] R.G. Loewy, N. Khader, Structural dynamics of rotating bladed disk assemblies coupled with flexible shaft motions, *AIAA Journal* 22 (9) (1984) 1319–1327.
[10] F. Wu, C.T. Flowers, A transfer matrix technique for evaluating the natural frequencies and critical speeds of a rotor with multiple flexible disks, *Journal of Vibration and Acoustics* 114 (1992) 242–248.
[11] M. Geradin, N. Kill, A new approach to finite element modeling of flexible rotors, *Engineering Computations* 1 (1984) 52–64.
[12] R.W. Stephenson, K.E. Rouch, Modeling rotating shafts using axisymmetric solid finite elements with matrix reduction, *Journal of Vibration and Acoustics* 115 (1993) 484–489.
[13] K.Y. Lam, C.T. Loy, Analysis of rotating laminated cylindrical shells by different thin shell theories, *Journal of Sound and Vibration* 186 (1) (1995) 23–35.
[14] G. Sun, P.N. Bennett, F.W. Williams, An investigation on fundamental frequencies of laminated circular cylinders given by shear deformable finite elements, *Journal of Sound and Vibration* 205 (3) (1997) 265–273.
[15] S.P. Singh, K. Gupta, Free damped flexural vibration analysis of composite cylindrical tubes using beam and shell theories, *Journal of Sound and Vibration* 172 (2) (1994) 171–190.
[16] H.L.M. Dos Reis, R.B. Goldman, Thin walled laminated composite cylindrical tubes—part I: boundary value problems—part II: bending analysis, *Journal of Composite Technology and Research* 9 (1987) 47–57.
[17] S.P. Singh, K. Gupta, Composite shafts rotordynamic analysis using a layerwise theory, *Journal of Sound and Vibration* 191 (5) (1996) 739–756.
[18] G. Jacquet-Richardet, G. Ferraris, P. Rieutord, Frequencies and modes of rotating flexible bladed disc–shaft assemblies: a global cyclic symmetry approach, *Journal of Sound and Vibration* 191 (5) (1996) 901–915.
[19] H. Irretier, G. Jacquet-Richardet, F. Reuter, Numerical and experimental investigations of coupling effects in anisotropic elastic rotors, *International Journal of Rotating Machinery* 5 (4) (1999) 263–271.
[20] D.L. Thomas, Dynamics of rotationally periodic structures, *International Journal for Numerical Methods in Engineering* 14 (1979) 81–102.
[21] R. Henry, G. Ferraris, Substructuring and wave propagation: an efficient technique for impeller dynamic analysis, *Journal of Engineering for Gas Turbine and Power* 106 (1) (1984) 2–10.
[22] R.R. Craig, M.C. Bampton, Coupling of substructures for dynamic analyses, *AIAA Journal* 6 (7) (1968) 1313–1319.
[23] E.S. Zorzi, J.C. Giordano, Composite shaft rotordynamic evaluation, *ASME Design, Engineering Division Conferences in Mechanical Vibration and Noise*, Cincinnati, USA, ASME paper, Vol. 85-det-114, 1985.
[24] M.S. Darlow, J. Creonte, Optimal design of composite helicopter power transmission shafts with axially varying fiber lay-up, *Journal of the American Helicopter Society* 40 (2) (1995) 50–56.
[25] S.P. Singh, H.B.H. Gubran, K. Gupta, Development in dynamics of composite material shafts, *International Journal of Rotating Machinery* 3 (1997) 189–198.
[26] K. Gupta, S.P. Singh, Damping measurements in fiber reinforced composite rotors, *Journal of Sound and Vibration* 211 (3) (1998) 513–520.
[27] O.A. Bauchau, Optimal design of high speed rotating graphite/epoxy shafts, *Journal of Composite Materials* 17 (3) (1983) 170–181.

[28] S. Ahmad, O.C. Zienkiewicz, B. Irons, Analysis of thick and thin shell structures by curved finite elements, *International Journal for Numerical Methods in Engineering* 2 (1970) 419–451.
[29] G. Jacquet-Richardet, P. Swider, Influence of fiber orientation on the dynamic behavior of rotating laminated composite blades, *Communications in Numerical Methods in Engineering* 13 (1997) 815–824.
[30] S.W. Tsaï, H.T. Hahn, *Introduction to Composite Materials*, Technomic, Lancaster, PA, 1980.
[31] ROTORINSA®, User Manual Version 2.1, Laboratoire de Mécanique des Structures, INSA Lyon, France, 1999.